Available online at www.sciencedirect.com
ScienceDirect
Proceedings of the Combustion Institute 000 (2018) 1–8
Proceedings of the Combustion Institute
www.elsevier.com/locate/proci

Counter rotating vortex pair structure in a reacting jet in crossflow

Vedanth Nair[a,*], Matthew Sirignano[a], Benjamin Emerson[a], Ben Halls[b], Naibo Jiang[c], Josef Felver[c], Sukesh Roy[c], Jim Gord[b], Tim Lieuwen[a]

[a] School of Aerospace Engineering, Georgia Institute of Technology, 270 Ferst Drive, Atlanta, GA 30332-0150, USA
[b] Air Force Research Laboratory, Wright Patterson Air Force Base, USA
[c] Spectral Energies LLC, Dayton, OH, USA

Received 30 November 2017; accepted 9 June 2018
Available online xxx

Abstract

This paper analyzes the time averaged flow structure of a reacting jet in cross flow (RJICF), emphasizing the structure of the counter-rotating vortex pair (CVP) by using simultaneous tomographic particle image velocimetry (TPIV) and hydroxyl radical planar laser induced fluorescence (OH-PLIF). It was performed to determine the extent to which heat release, and the associated effects of gas expansion and baroclinic vorticity production, impact the structure of the CVP. These results show the clear presence of a CVP in the time averaged flow field, whose trajectory lies below the jet centerline on either side of the centerplane. Consistent with other measurements of high momentum flux ratio JICF in nonreacting flows, there is significant asymmetry in strength of the two vortex cores. The strength and structure of the CVP was quantified with vorticity and swirling strength (λ_{ci}), showing that some regions of the flow with high shear are not necessarily accompanied by large scale bulk flow rotation and vice-versa. The OH PLIF measurement allows for correlation of the flame position with the dominant vortical structures, showing that the leeward flame branch lies slightly above, as well as, in the region between the CVP cores.

Keywords: Jet in cross flow; Tomographic particle image velocimetry; Counter-rotating vortex pair

---

1. Introduction

The jet in cross flow (JICF) is an important flow configuration that is of technological interest due to its applicability in staged combustion for both fuel and air injection. The flow structures in a JICF enables rapid mixing between the jet and crossflow contents [1] through several large scale, coherent vortical structures forming a highly three-dimensional flow-field, both instantaneously and on average. The four types of coherent structures in the non-reacting JICF [2] consist of: (i) horseshoe vortices (HV), (ii) upright wake vortices (WV), (iii) the counter-rotating vortex pair (CVP), and (iv) shear layer vortices (SLV). Of these structures, the CVP is the dominant vortical structure in the wake

---

[*] Corresponding author.
E-mail address: vnair36@gatech.edu (V. Nair).

https://doi.org/10.1016/j.proci.2018.06.059
1540-7489

Please cite this article as: V. Nair et al., Counter rotating vortex pair structure in a reacting jet in crossflow, Proceedings of the Combustion Institute (2018), https://doi.org/10.1016/j.proci.2018.06.059

of the jet [3] and contributes in a large part to the enhanced mixing characteristics of the jet with the cross flow [4].

The formation of the CVP, and it's structure, has been linked to the periodic vortex ring rollup from the jet shear layers [5]. These shear layers originate at the jet exit and form the shear layer vortices (SLVs) which distort and fold from their cylindrical form due to the effect of the crossflow [6], and the mutual self-induction of vorticity from one part of the SLV to the other [7–10]. However, while the CVP is clearly present in the time-averaged flow, its presence is much less obvious in instantaneous snapshots of the flow-field, since the folding and tilting of successive vortex sheets contributes to the net circulation of the CVP [6,10].

The non-reacting JICF structure is dependent on parameters including the crossflow Reynolds number Re_∞, jet momentum flux ratio, $J = \rho_j u_j^2/\rho_\infty u_\infty^2$, and the jet density ratio, $S = \rho_j/\rho_\infty$ [7,8]. Experimental characterization of cross sectional slices of the non-reacting CVP have been used to measure the time-averaged flow-field [3,7]. Quantitative velocity data for cross-sections of the CVP have been performed with probes [11] and planar PIV [12]. Planar PIV measurements suffers from the inability to quantitatively obtain a three-dimensional velocity gradient field, which is important for visualizing a highly three-dimensional structure such as the CVP. The only study we are aware of that used full volumetric, 3D velocity measurements was done by Cambonie et al. [13] using volumetric 3D Particle Tracking Velocimetry (3DPTV) to analyze the mean flow of a transverse water jet. Their study analyzed the three-dimensional structure of the CVP field and tracked the trajectory of the vortex cores to obtain scaling laws with respect to different values of J, jet diameter (d_j) and the boundary layer thickness (δ).

In the case of RJICF, the limited data available suggests that reactions have a minimal impact on the time-averaged jet trajectory [12,14]. The behavior and the structure of the CVP in the presence of exothermic reactions have been investigated by fewer studies. The incompressible vortex model developed by Karagozian [15] assumes that the RJICF flow-field will be similar to the non-reacting case and investigates the effects of the entrainment rate due to the CVP on the flame length and shape. Similarly, many experimental RJICF studies implicitly assume its existence, but the characterization of its structure and location is incomplete.

There is good reason to expect that combustion could both qualitatively and quantitatively influence the CVP in the RJICF through both gas expansion and baroclinic vorticity effects. For example, there is no mechanism for vorticity generation in the interior of the flow in the iso-density JICF. All vorticity in the flow originates either from the boundary layers in the jet or bounding walls, and is subsequently redistributed and reoriented in the flow domain. In contrast, in the reacting flow, vorticity can be generated via the baroclinic mechanism or damped via gas expansion modifying the interactions of one region of vorticity with another. For example, in two-dimensional reacting wakes (with two shear layers), combustion-induced gas expansion materially alters the degree of interaction of the shear layers and suppresses the formation of the Von Karman vortex street [16].

This study aims to investigate the time-averaged flow field structures present in the RJICF field - primarily the structure and the evolution of the CVP. Similar to the study of Coriton et al. [17], which employed Tomographic Particle Image Velocimetry (TPIV) to resolve three-dimensional flow structures in a lifted jet flame, the study employs 10KHz high speed TPIV. The volume over which the PIV vectors were evaluated was significantly larger than previous studies to capture the extent of the CVP structures. The ability to fully compute gradients in all three directions, which is not possible in planar or stereo-PIV vector fields, was utilized to visualize gradient dependent quantities (i.e., three-dimensional vorticity), and to resolve the three-dimensional flow structures. Simultaneous OH-PLIF was used to investigate the center-plane flame structure. Although the influence of the flow-field structures on flame structure and stabilization is thought to be significant for RJICF [10,12], the limitations of planar PIV diagnostics utilized by most experimental studies on both fuel and premixed jets [14,18,19], limit the investigation of the flame-flow interaction to the center-plane flow-field. The only work to provide a three-dimensional view of the flame structure as well as the associated flow-field is the DNS study of Grout et al. [20]. The current work aims to provide experimental insights into the structure of the time averaged, three-dimensional flow field, and the associated flame position. Key questions include: (i) Is the structure of the CVP fundamentally altered in the presence of combustion? (ii) Where does it sit with respect to the flame?

2. Main body

2.1. Experimental setup

The setup consists of a lean, swirling main burner which burns methane and air (preheated to 575 K) at an equivalence ratio, $\Phi_{HE} = 0.4$. The hot combustion products pass through a ceramic honeycomb flow conditioning section to obtain a uniform non-swirling crossflow at a temperature, $T_\infty = 1450$ K and $Re_\infty = 6400$. The test section contains a flush mounted methane jet using a ceramic nozzle contoured to obtain a top-hat velocity profile [8]. The test section has dimensions of $189d_j$ (length) × $25d_j$ (width) × $42d_j$ (height),

Please cite this article as: V. Nair et al., Counter rotating vortex pair structure in a reacting jet in crossflow, Proceedings of the Combustion Institute (2018), https://doi.org/10.1016/j.proci.2018.06.059

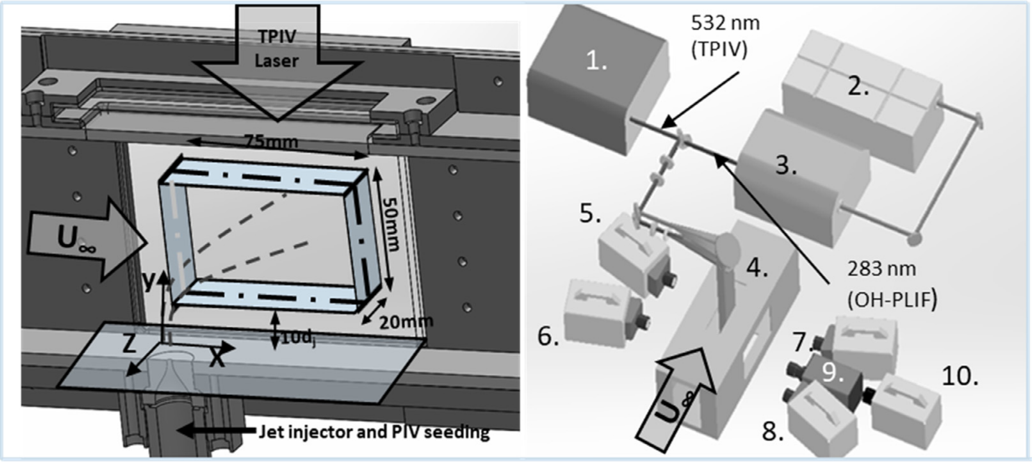

Fig. 1. (left) Schematic of the test-section with reconstructed PIV volume; (right) Schematic of the laser diagnostic setup; 1- High speed TPIV laser, 2- EdgeWave Nd:YAG Laser, 3-SirahCredo Tunable Dye Laser, 4-Test section, 5-FastCam SA-Z#1 (TPIV), 6-FastCam SA-Z#2 (TPIV), 7-FastCam SA-Z#3 (TPIV), 8-FastCam SA-Z#4 (TPIV), 9-LaVision HiCATT intensifier, 10-FastCam SA-X (OH-PLIF).

with optical access up to 50d_j downstream of the jet, where $d_j = 3$ mm. A jet momentum flux ratio (J) of 90 ($Re_j = 8000$) was used to obtain a highly penetrating jet fixed near the center of the viewable volume, as well as a value that substantially exceeds the globally unstable bifurcation boundary, $J \sim 10$, noted by Megerian et al. [8].

The schematic of the diagnostic setup used in this study is shown in Fig. 1 above. For TPIV measurements, a quasi-continuous burst-mode (QCBM) laser (QuasiModo, Spectral Energies LLC) is used [21,22]. The laser produces a high-energy double pulse train of 532 nm pulses of width 10 ns, with a separation of 40 µs (between the double pulses) while operating at 10 KHz. The burst duration for each measurement set lasts 10 ms to yield 75 image pairs per burst, repeated every 12 s a total of 7 times. The pulse energy is maintained at 200 mJ per pulse to ensure sufficient illuminating intensity over the entire PIV volume. Since the laser energy is diffused over such a large volume, 3–5 micron TiO_2 particles were used in both the jet and crossflow to achieve a sufficient signal to noise ratio. The illuminated volume is controlled by using a square slit which positions the volume of $44d_j$ (length) × $6.66d_j$ (width) × $42d_j$ (height) so that its centerplane coincides with the jet centerplane and it illuminates a distance of up to $40d_j$ downstream of the jet to capture the CVP. The images were captured by 4 high speed CMOS cameras (Photron SA-Z) operating at 20 kHz in frame-straddling mode with full resolution (1024 × 1024 pixels). The cameras used a Nikon 55 mm camera lens (f/4.0) and their focal plane was aligned using Scheimfplug adapters, with camera 1 and 2 oriented at an angle of 10° while camera 3 and 4 were oriented at an angle of 30° to the centerplane normal. A 9 nm FWHM band-pass optical filter was used centered at 532 nm.

The OH-PLIF measurements used a frequency-doubled Nd:YAG laser (Edgewave InnoSlab IS811-E) operating at 10 kHz as the pump laser, and a frequency-doubled tunable dye laser (Sirah Credo LG24) operating with a Rhodamine 6 G dye solution. The UV output of 0.16 mJ/pulse at 283 nm was tuned to the $Q_1(9)$ transition of OH in the (1,0) band of the $A^2\Sigma^+$- $X^2\Pi$ system. The beam was expanded into a sheet measuring 0.4 mm placed at the center of the illuminated TPIV volume such that the flame at the centerplane of the methane jet would be captured. The OH-fluorescence was captured by a high-speed CMOS camera (Photron SA-X) which used a high-speed image intensifier (LaVision HS-IRO) and no filter to maximize the signal to noise. The OH-PLIF laser pulse was synchronized along with the TPIV system with the image being acquired in the middle of the TPIV pulse doublet.

2.2. Methodology

The image pairs captured from the TPIV technique were processed using the Davis 8.1.6 software from LaVision. The image were preprocessed by normalizing the instantaneous images with the average laser intensity to account for the pulse to pulse intensity variation. The scaled mean intensity image was then subtracted recursively from the instantaneous images to remove the reflections and static noise, and the resulting images were smoothed with a 3 × 3 px^2 Gaussian filter. The images were then used to refine the calibration by the

Please cite this article as: V. Nair et al., Counter rotating vortex pair structure in a reacting jet in crossflow, Proceedings of the Combustion Institute (2018), https://doi.org/10.1016/j.proci.2018.06.059

volume self-calibration procedure [23] with an average error in the centerplane of 0.062 pixels and disparity vector length of 0.4–0.8 pixels. The preprocessed images were then used to reconstruct the particle distribution volume [24]. The reconstructed volume measured 75 × 50 × 20 mm^3 resulting in 664 × 449 × 180 voxels and is displayed in Fig. 1. This region was chosen to capture the main structure of the CVP which extends significantly downstream of the jet, and to minimize the influence of wall reflections. The particle displacements were determined by using multi-pass cross-correlation with an interrogation volume of dimensions 48 × 48 × 48 with 75% overlap of neighboring regions, resulting in a final vector spacing of 1.37 vectors/mm. Vector post processing was done iteratively to remove spurious outliers and vectors with a correlation value lower than 0.1. The resultant field was smoothed with a 3 × 3 × 3 pt Gaussian filter.

The Stokes number, i.e., the ratio of characteristic particle relaxation time and CVP rotation time was estimated assuming a characteristic particle frequency scale as 10 kHz (using the formula by Melling [25]) and that the CVP Strouhal number, $St = f_0 d_j / u_j = 0.016$ [26]. Thus, the Stokes number associated with the CVP, $Stk_{CVP} \sim 0.042$, implies that the particles closely follow the CVP motions. Spatially, the vector resolution is roughly $\sim O(dj)$, while the CVP is a large scale structure known to extend downstream up to $40d_j$ and with a width of nearly $10d_j$ at a distance of $10d_j$ from the jet [7]. Thus, the gradients in the x-direction associated with the dominant vorticity associated with the time averaged CVP structure is sufficiently captured, but not the fine scale SLV structures.

The time averaged flow-field for this data set was created by averaging over the 7 pulse bursts of a total of 525 vector fields. The correlation coefficient for most vectors in the crossflow were around 0.6–0.7 while the vectors near the jet core were around 0.3–0.4. This variation in values occurs because of the significant differences in particle motion with location. Random uncertainties in velocity are estimated to be much larger than bias errors [27] and were calculated to range from 4% (in the jet core) to 2% (in the crossflow) with the outer planes having a higher uncertainty, using the relation $U_{\bar{u}} = \sigma_u / N^{0.5}$ [28] where σ_u is the standard deviation of the velocity and N, the number of samples . To establish convergence, the mean velocity $\bar{u}$ was calculated with $N = 400$ and $N = 525$ samples and the average RMS was less than 0.1%.

The OH-PLIF images were processed by normalizing the images to the instantaneous laser sheet intensity and an edge preserving filter was used to smooth out some of the noise and retain the sharp gradients at the flame edge. The intensity range of noise was found to be between 0-10% max PLIF signal ($I_{\max}$), and regions of elevated temperature where elevated OH levels persist, lay between 20-100% $I_{\max}$. To obtain the threshold, Otsu's method was used for each instantaneous image. To test the sensitivity of the results the threshold was varied by 20% resulting in a 2% area reduction for the windward flame edge and a 10% reduction in area in the leeward flame. This difference is due to the much higher scalar dissipation rate and associated OH/temperature gradients on the windward side than the leeward side. Since a filter was not used for the PLIF signal, scattered light from large TPIV particles were filtered out of the binarized image using an area filter and the resulting image was used to obtain the instantaneous flame edges. The binarized images were also averaged to obtain the flame probability distribution field, p_τ, which quantifies the probability of high-temperature combustion products being present at a given location.

2.3. Results

Figure 2 shows a schematic of the SLV rollup phenomenon along with representative instantaneous images which overlay the velocity field along the center jet x-y plane, the z-vorticity (ω_Z), and the regions of elevated OH. The SLV vortex rings originate at the jet exit and, distort and bend [6] as they advect downstream, creating vortex pairs which can be visualized in the centerplane as a train of alternating positive and negative vortical structures in the windward and leeward side of the jet. The OH PLIF clearly shows that the windward side of the flame is lifted, while the leeward is attached to the jet exit, similar to the flames analyzed by Steinberg et al. [18] for a hydrogen fuel jet, Wagner et al. [19] for a premixed ethylene jet, and Sullivan et al. [14] for a methane fuel jet. Similar to prior observations, the elevated OH region is much thinner on the windward side than the leeward side, due to higher scalar dissipation rates causing sharper temperature gradients.

To visualize the three-dimensional mean flow-field, we use the swirling strength (λ_{ci}) field [29], which, is the magnitude of the complex component of the conjugate eigenvalue pair from the velocity gradient tensor ($\nabla \vec{U}$). This scalar field is computed from the time-averaged flow-field to observe the presence of the CVP. In Fig. 3, the two iso-swirling strength surfaces are plotted, with the color of the surface indicating the value of the axial vorticity to show the two counter-rotating structures. Note that the negative ω_x structure is larger in size and magnitude than the positive one. This result is consistent with other studies that have similarly noted asymmetries in the time averaged CVP cross-section for high J nonreacting jets [7,30]. The jet centerline marked in the figure was obtained by applying the Rd_j scaling introduced by Pratte et al. [31], $y/Rd_j = A(x/Rd_j)^b$, on the maximum velocity streamline, obtaining the scaling coefficients $A = 1.65$ and $b = 0.33$ which lie within the

Please cite this article as: V. Nair et al., Counter rotating vortex pair structure in a reacting jet in crossflow, Proceedings of the Combustion Institute (2018), https://doi.org/10.1016/j.proci.2018.06.059

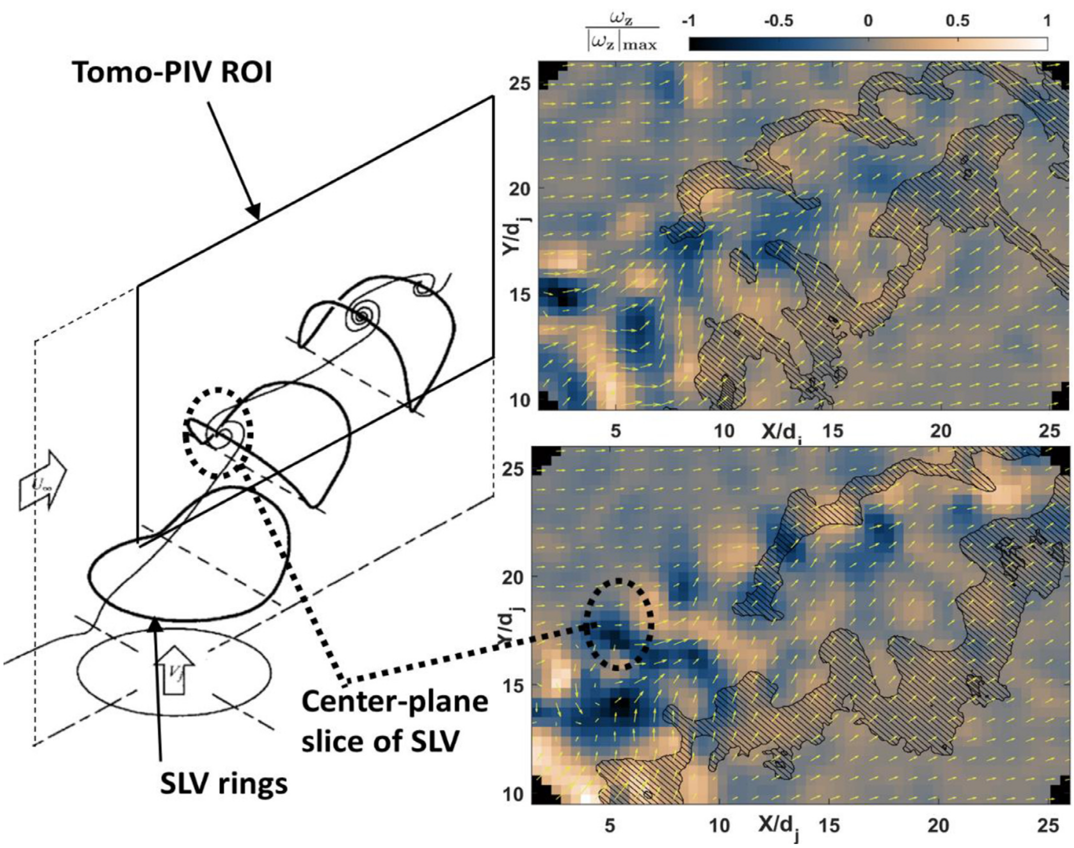

Fig. 2. (left) Schematic of vortex rollup and distortion [6] with PIV region of interest (ROI) demarcated; (right) Representative instantaneous overlay(s) of out of plane vorticity (ω_Z) (color scale), velocity vectors, and elevated OH PLIF regions (hashed)($|\omega_Z|_{\max} = 7893.6\ \mathrm{s}^{-1}$).

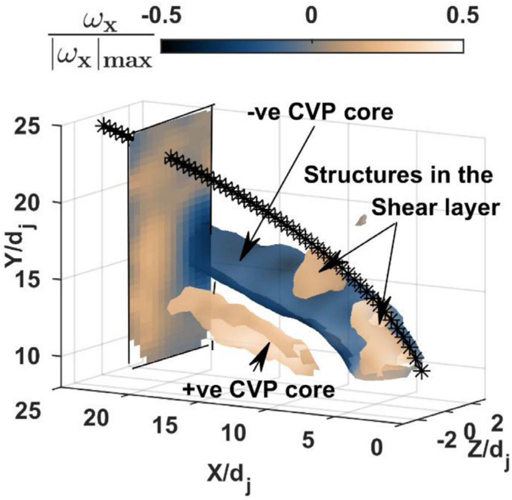

Fig. 3. Three-dimensional plot showing iso-surfaces of $\lambda_{ci} = 0.4$, colored with the normalized vorticity in the axial direction (ω_x), to demonstrate the two different CVP branches and the jet velocity centerline (*). ($\omega_{x,max} = 1253\ \mathrm{s}^{-1}$).

ranges noted in literature [1]. Thus, the CVP lies well below the jet core, similar to the observations for non-reacting jets [13,32].

High shear in this flowfield makes coherent structure identification using vorticity problematic [29]. To illustrate, Fig. 4 shows different views of the vorticity, swirling strength (defined earlier) and shear strength $||S||$. Shear is defined as $||S|| = [tr(S_{ij}S'_{ij})]^{0.5}$ [29] where S_{ij} is the symmetric part of the velocity gradient tensor $\nabla\vec{U}$. As the planar slices demonstrate, regions of bulk rotation (λ_{ci}) and shear $||S||$ do not occur at the same location. The CVP, also associated with bulk flow rotation, can be seen in all the planes. In addition, planes 1 and 2 show other concentrated vorticity regions, where the the shear strength dominates. This is more apparent from the central schematic which shows shear iso-surfaces ($||S||/||S||_{\max} = 0.4$) near the base of the CVP. Comparing this with the schematic of SLV rollup given in Fig. 2, suggests that elevated shear could be linked to the distortion of the SLV rings, since the dissipation of the shear occurs spatially in the same location as the CVP strengthens and becomes the dominant

Please cite this article as: V. Nair et al., Counter rotating vortex pair structure in a reacting jet in crossflow, Proceedings of the Combustion Institute (2018), https://doi.org/10.1016/j.proci.2018.06.059

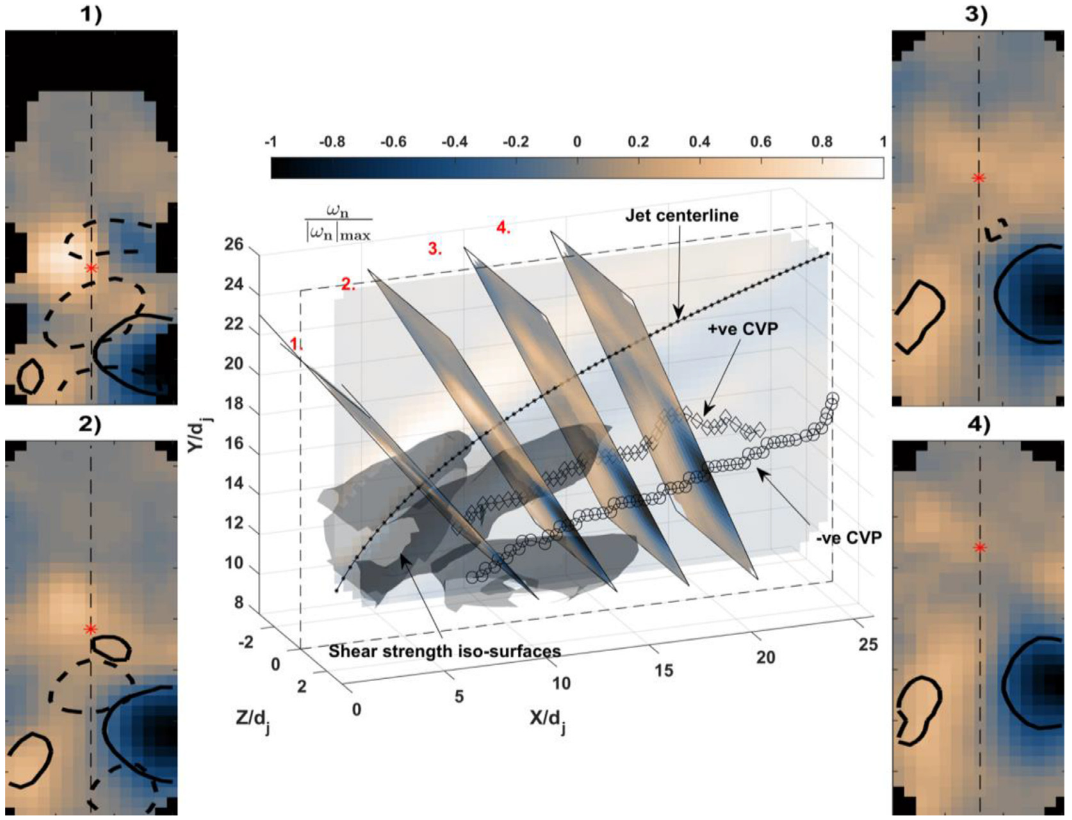

Fig. 4. Three-dimensional plot of out of plane vorticity from four planes normal to the jet trajectory at $s/dj = 10, 14, 17.5, 22$ where s is the coordinate along the jet centerline; positive ('◊') and negative ('o') CVP branches are marked along with the jet centerline trajectory ('.'); Plot of out of plane vorticity with iso-lines of $\lambda_{ci} / \lambda_{ci,max} = 0.25$ (solid), $\|S\|/\|S\|_{max} = 0.25$ (dashed) plotted for each plane; point at which each plane intersects with the jet core is marked with a red asterisk '*'. ($\lambda_{ci,max} = 2227$ s^{-1}; $\|S\|_{max} = 3368$ s^{-1}; $|\omega_n|_{max} = 1525$ s^{-1}) .

vortical structure. Also indicated in the center figure is the trajectory of the two branches of the CVP, corresponding to the center of the two regions of high λ_{ci} through planes perpendicular to the jet trajectory. Noting that the transverse position (z-direction) of the CVP centers remained relatively constant, the two trajectories were fit using a similar Rd_j scaling with coefficients, $A_{pos} = 1.19$, $b_{pos} = 0.35$ and for the other branch $A_{neg} = 1.13$, $b_{neg} = 0.3$.

The strength of the CVP is tracked by measuring the average circulation (Γ), calculated as the integral of the net vorticity, as well as the net swirling strength (A_λ), calculated as the integral of the net swirling strength contained in the planar cross section of the CVP core of each vortex structure along each plane perpendicular to the centerline. The coordinate system along the CVP trajectories (s) starts nearly 15 diameters downstream of the jet exit due to the planes cutting through the CVP in the near field lying partially outside the measurement volume. The peak in swirling strength in the near field was also noted in the case of non-reacting JICF [13] and is noted in the same spatial region where the shear structures noted in Fig. 4 stop being dominant. From Fig. 5, the comparison in strength of the two separate branches is apparent as well as the gradual reduction in both vorticity and swirling strength as we move downstream due to the dissipation of this structure.

To compare the time-averaged flame and jet structure, Fig. 6 plots the time averaged velocity, vorticity, and two iso-p_τ contours on the jet centerplane, in addition to fits for the jet and CVP centerlines. The out of plane vorticity in the figure, (ω_z), clearly shows the presence of the windward and leeward shear layers lying on either side of the jet centerline. The p_τ contours in the figure shows that the leeward flame signal lies essentially in the region between the CVP vortices. This is noted in DNS data [20], where the peak heat release was found to lie in the centerplane slightly above and between the CVP structure. This shows that the typically attached leeward flame observed in these

Please cite this article as: V. Nair et al., Counter rotating vortex pair structure in a reacting jet in crossflow, Proceedings of the Combustion Institute (2018), https://doi.org/10.1016/j.proci.2018.06.059

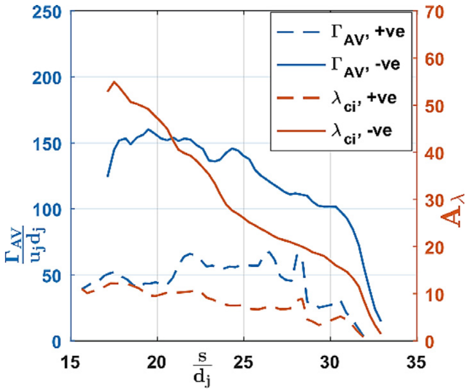

Fig. 5. Plot of circulation (Γ) and net swirling strength (A_λ) along the CVP trajectory (s).

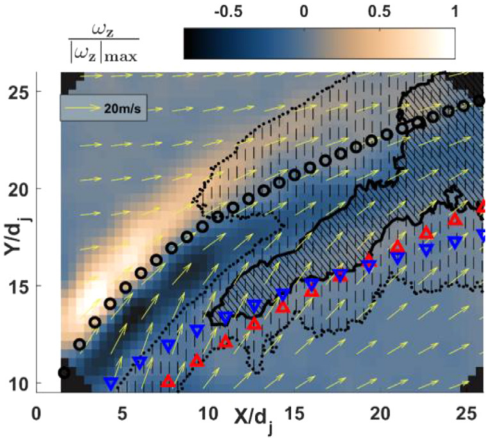

Fig. 6. Time-averaged vorticity field and velocity vectors overlaid (1 vector per 4 × 4 grid); Iso-contours mark regions of $p_\tau = 0.15$ (vertical hashing) and $p_\tau = 0.25$ (oblique hashing); The jet centerline ('o') and fit for the+ ve ('Δ') and −ve ('∇') CVP trajectories have been marked on it. ($|\omega_z|_{max} = 1525\ s^{-1}$).

configurations is a consequence of flame stabilization due to the CVP and the behavior of the CVP can influence both post-flame mixing as well as flame liftoff height.

3. Conclusion

This study presents the first application of three-dimensional flow measurements using TPIV to gain insight into the flow topology of a reacting JICF. The data allowed simultaneous comparison of well documented flow features, i.e., the instantaneous centerplane vorticity showing the advecting SLVs, with a novel measurement of the three-dimensional mean flow to understand if and how the CVP is formed from the SLVs in reacting flows. This also allowed us to analyze the full velocity gradient tensor, and to determine the dominant directions of flow distortion. To this effect, the mid field ($10 < s/d_j < 20$) topology is dominated by shear (associated with streamwise vorticity; not out of plane, spanwise vorticity, which presumably dominates in the very near field, upstream of the measurement window), believed to be due to the turning and distortion of the SLV rings. The far field ($s/d_j > 20$) is dominated by the streamwise bulk flow rotation of the CVP, demonstrating the spatial locations along the jet where the CVP becomes dominant. A prominent question motivating this study was the extent to which combustion effects on vortex interactions (e.g., gas expansion/baroclinic torque) materially alter SLV ring interactions that leads to CVP formation. The topological similarity to the well-documented non-reacting flowfield suggests that combustion effects on SLV structures/interactions are not significant enough to prevent their formation into the CVP. Lastly, the combustion products centerplane distribution emphasizes the importance of the CVP on the axial location of reaction initiation/flame stabilization. Specifically, consistent with Grout et al. [20], the location where significant reaction is present the majority of the time (i.e., high p_τ values) is on the leeward side of the jet and occurs at a location not coincident with the jet exit, nor the low velocity shear layers, but along the CVP (see Fig. 6).

Acknowledgments

This manuscript was cleared for public release by the Air Force Research Laboratory (#88ABW-2017-5780). This research was supported by the University Turbine Systems Research (Contract no. DE-FE0025344), contract monitor Dr. Mark Freeman, Air Force Research Laboratory (Contract no. FA8650-15- D -2518 and FA8650-18-C-2001) and the National Science Foundation (Contract no. 1705649), contract monitor, Dr. Song-Charng Kong.

Supplementary materials

Supplementary material associated with this article can be found, in the online version, at doi:10.1016/j.proci.2018.06.059.

References

[1] A.R. Karagozian, *Prog. Energy Combust. Sci.* 36 (5) (2010) 531–553.
[2] T. Fric, A. Roshko, *J. Fluid Mech.* 279 (1994) 1–47.
[3] T. Fric, A. Roshko, Structure in the near field of the transverse jet, 7th Symposium on Turbulent Shear Flows, 1989.

Please cite this article as: V. Nair et al., Counter rotating vortex pair structure in a reacting jet in crossflow, Proceedings of the Combustion Institute (2018), https://doi.org/10.1016/j.proci.2018.06.059

[4] L. Gevorkyan, T. Shoji, D.R. Getsinger, O.I. Smith, A.R. Karagozian, *J. Fluid Mech.* 790 (2016) 237–274.
[5] J. Andreopoulos, W. Rodi, *J. Fluid Mech.* 138 (1984) 93–127.
[6] R.M. Kelso, T. Lim, A. Perry, *J. Fluid Mech.* 306 (1996) 111–144.
[7] D.R. Getsinger, L. Gevorkyan, O.I. Smith, A.R. Karagozian, *J. Fluid Mech.* 760 (2014) 342–367.
[8] S. Megerian, J. Davitian, L.S. de, B. Alves, A.R. Karagozian, *J. Fluid Mech.* (2007) 593.
[9] S. Peterson, M. Plesniak, *J. Fluid Mech.* 503 (2004) 57–91.
[10] L. Cortelezzi, A.R. Karagozian, *J. Fluid Mech.* 446 (2001) 347–373.
[11] R. Fearn, R.P. Weston, *AIAA J.* 12 (12) (1974) 1666–1671.
[12] E.F. Hasselbrink, M.G. Mungal, *J. Fluid Mech.* (2001) 443.
[13] T. Cambonie, N. Gautier, J.L. Aider, *Exp. Fluids* 54 (3) (2013).
[14] R. Sullivan, B. Wilde, D.R. Noble, J.M. Seitzman, T.C. Lieuwen, *Combust. Flame* 161 (7) (2014) 1792–1803.
[15] A.R. Karagozian, *AIAA J.* 24 (9) (1986) 1502–1507.
[16] B. Emerson, J. O'Connor, M. Juniper, T. Lieuwen, *J. Fluid Mech.* 706 (2012) 219–250.
[17] B. Coriton, A.M. Steinberg, J.H. Frank, *Exp. Fluids* 55 (6) (2014) 1743.
[18] A.M. Steinberg, R. Sadanandan, C. Dem, P. Kutne, W. Meier, *Proc. Combust. Inst.* 34 (2013) 1499–1507.
[19] J.A. Wagner, S.W. Grib, M.W. Renfro, B.M. Cetegen, *Combust. Flame* 162 (10) (2015) 3711–3727.
[20] R.W. Grout, A. Gruber, C.S. Yoo, J.H. Chen, *Proc. Combust. Inst.* 33 (1) (2011) 1629–1637.
[21] J.D. Miller, J.B. Michael, M.N. Slipchenko, S. Roy, T.R. Meyer, J.R. Gord, *Appl. Phys. B* 113 (1) (2013) 93–97.
[22] S. Beresh, S. Kearney, J. Wagner, et al., *Measur. Sci. Technol.* 26 (9) (2015) 095305.
[23] B. Wieneke, *Exp. Fluids* 45 (4) (2008) 549–556.
[24] G.E. Elsinga, F. Scarano, B. Wieneke, B.W. van Oudheusden, *Exp. Fluids* 41 (6) (2006) 933–947.
[25] A. Melling, *Measur. Sci. Technol.* 8 (12) (1997) 1406.
[26] S. Bagheri, P. Schlatter, P.J. Schmid, D.S. Henningson, *J. Fluid Mech.* 624 (2009) 33.
[27] B. Wieneke, *Measur. Sci. Technol.* 26 (7) (2015) 074002.
[28] A. Sciacchitano, B. Wieneke, *Measur. Sci. Technol.* 27 (8) (2016) 084006.
[29] J. Jeong, F. Hussain, *J. Fluid Mech.* 285 (1995) 69–94.
[30] S.H. Smith, M.G. Mungal, *J. Fluid Mech.* 357 (1998) 83–122.
[31] B.D. Pratte, W.D. Baines, *J. Hydraul. Div.* 93 (6) (1967) 53–64.
[32] S. Muppidi, K. Mahesh, *J. Fluid Mech.* 530 (2005) 81–100.

Please cite this article as: V. Nair et al., Counter rotating vortex pair structure in a reacting jet in crossflow, Proceedings of the Combustion Institute (2018), https://doi.org/10.1016/j.proci.2018.06.059